Title
Tough, dendrite-suppressing and anti-freezing hydrogels electrolyte for zinc-ion batteries operating in harsh conditions

Author
Wang, Ta-Wei

Publication Date
2022

Peer reviewed|Thesis/dissertation

UNIVERSITY OF CALIFORNIA

Los Angeles

Tough, Dendrite-Suppressing and Anti-Freezing Hydrogels Electrolyte for Zinc-Ion Batteries operating in harsh conditions

A thesis submitted in partial satisfaction

of the requirements for the degree Master of Science

in Materials Science and Engineering

by

Ta-Wei Wang

2022

ABSTRACT OF THE THESIS

Tough, Dendrite-Suppressing and Anti-Freezing Hydrogels Electrolyte for Zinc-Ion Batteries operating in harsh conditions

by

Ta-Wei Wang

Master of Science in Material Science and Engineering

University of California, Los Angeles, 2022

Professor Ximin He, Chair

Aqueous zinc-ion batteries (AZIBs) have been considered as promising candidates for large-scale energy storage due to their high theoretical capacities, low cost, and high safety. However, the leakage and dendrite growth at extreme working conditions seriously limits their application. Herein, an anti-freezing, dendrite-suppressing, and tough hydrogel electrolyte is developed by using polyvinyl alcohol (PVA) as a polymer framework, soaked into a zinc sulfate ($ZnSO_4$)/dimethyl sulfoxide (DMSO)/H_2O electrolyte solution.

The thesis of Ta-Wei Wang is approved.

Yu Huang

Aaswath Pattabhi Raman

Ximin He, Committee Chair

University of California, Los Angeles

2022

Table of Contents

List of Figures

List of Tables

Acknowledgements

I would like to express gratitude to Dr. He for her guidance and show my appreciation towards members of the He Lab for their assistance.

I would also like to thank Dr. Yu Huang and Dr. Aaswath Raman for being on my committee and reviewing this work.

Lastly, I am grateful for the love and support that my family, friends have given me.

1 Introduction

Lithium-ion batteries dominate the power source market for their high energy density and long lifespan [1]. However, drawback such as high cost, flammability, and toxicity, limit their potential as next-generation power sources, such as grid storage and wearable electronics [2]. Aqueous zinc-ion batteries (AZIBs) have attracted great attention in recent years owing to their high safety, low cost, resource abundance, and high theoretical capacity [3]–[5]. Nevertheless, AZIBs using traditional liquid electrolytes still suffer from several issues including leakage, dendrite growth, hydrogen evolution, byproduct formation, and cathode dissolution [6][7]. Hydrogel electrolytes, crosslinked polymer network swollen with aqueous solution, can address these problems through the polymer-ion-water interactions as well as enhanced mechanical properties, which allow them to endure large mechanical deformation while still effectively separating the cathode and anode to prevent shorting [7]. It is also essential for them to exhibit anti-freezing behavior to inherently adapt low-temperature environments, without the usage of bulky and costly engineering designs to heat the batteries. To deal with this freezing issue, high contents of salts and organic solvents have been widely applied to enhance the anti-freezing property of hydrogel electrolytes[8]–[13]. However, the proposed strategies faced several drawbacks. For example, Bis(trifluoromethane)sulfonimide ($LiN(CF_3SO_2)_2$) can be

used as an anti-freezing component. However, it is expensive and can't contribute any zinc ions [14]. Adding organic solvents (e.g., glycerol) allows the hydrogel to remain soft and flexible at -35℃ and shows a good cycling performance at low temperature [15]. Unfortunately, the mechanical properties of that hydrogel are insufficient (Ultimate tensile strength: 120kPa). Therefore, developing a hydrogel electrolyte by using low concentration salt and organic additives to offer satisfactory mechanical properties as well as ionic conductivity at subzero temperature is of great importance.

Wu et al. demonstrated an anti-freezing and dendrite-suppressing liquid electrolyte by adding dimethyl sulfoxide (DMSO) into an aqueous $ZnSO_4$ solution. Because the DMSO has strong hydrogen bond interaction with water, the free water molecules concentration inside the electrolyte solution can be decreased with increasing DMSO concentration and the freezing temperature can be lowered. Also, Zn deposition preferred to form towards the more electrochemical stable (002) basal plane in such an environment, which reduces the dendritic growth [16]. Even though the abovementioned liquid electrolytes have high ionic conductivity and excellent cycling performance at subzero temperature, they are still in the liquid state, which causes poor mechanical strength and leakage issues.

Inspired by this study, herein we introduced an anti-freezing, dendrite suppressing, and mechanically strong hydrogel electrolyte, by using polyvinyl alcohol (PVA) as the

polymer backbone and $ZnSO_4$/DMSO/H_2O as the electrolyte solution (Figure 1a). PVA is chosen because the Hofmeister effect can be utilized to tune the mechanical properties of it and $ZnSO_4$ can salting-out PVA to enhance its mechanical properties [17]. Attributed to the salting-out effect of $ZnSO_4$, the tensile strength and toughness of our hydrogel electrolytes can reach 5 times and 50 times higher than a commercial separator with a liquid electrolyte. Also, due to the strong hydrogen bonds between DMSO and H_2O, the gel can remain unfrozen at -20℃ when 30wt% DMSO is added. Furthermore, DMSO can regulate the zinc ion deposition to form the Zn (002) texture and suppress the dendrite formation. Benefitted from the abovementioned advantages, Zn/PANi batteries with our hydrogel electrolyte can offer a high-rate performance as well as long-term stabilities at both 25℃ and -20℃.

2 Material and Methods

2.1 Materials

Dimethyl sulfoxide (DMSO) (Fisher scientific, >-99.7%). Poly(vinyl alcohol) (PVA) (weight-average molecular weight (Mw) of 89-98 kDa and 195kDa; degree of hydrolysis of 99%), Zinc sulfate heptahydrate ($ZnSO_4 \cdot 7H_2O$) (ACS reagent, 99%), Zinc perchlorate hexahydrate ($Zn(ClO_4)_2 \cdot 6H_2O$), Zinc Acetate dihydrate ($Zn(CH_3COO)_2 \cdot 2H_2O$) (ACS reagent, ≥98%), Zinc chloride ($ZnCl_2$) (reagent grade, ≥98%), Aniline (ACS reagent, ≥99.5%), Ammonium persulfate (ACS reagent, ≥98%), were all purchased from Sigma Aldrich. Hydrochloric acid (HCl) (36%, technical, Thermo Scientific™) was purchased form Fisher scientific. Commercial glass fiber (Whatman GF/C ™). Carbon cloth (ELAT-Hydrophilic Plain Cloth, 1591002) was purchased from Fuel Cell store.

2.2 Preparation of PVA precursors

PVA precursor solutions were prepared by adding 10 wt% of PVA powder in water and DMSO respectively before heating up to 95℃ and stirring for 2 hours.

2.3 Preparation of DMSO/H_2O/$ZnSO_4$ solutions

DMSO volume ratios in DMSO/H_2O solutions of 0%, 10%, 20%, 30%, 40%, 50%, and 60% were prepared. Afterward, 2M $ZnSO_4 \cdot 7H_2O$ salt was added to the above solutions to acquire the solutions.

2.4 Preparation of PANi Cathode

0.365mL aniline monomer was added into 15mL 1M HCl solution with continuous stirring and then carbon cloth pieces (3x3cm) were dipped into the solution and stored in the refrigerator at 4℃ for 1h. Next, 5mL 1M HCl solution containing 0.228g APS was also prepared and stored in the refrigerator for 1h. The two solutions were then mixed and placed at RT for 3h. The polymerization occurred during this time and the whole solution became dark green. The carbon cloth pieces were washed with deionized water, then with ethanol, and then dried at 60℃ in a vacuum oven overnight. The PANi/Carbon Cloth pieces were then cut into 1cm x 1cm pieces for use. The mass loading of PANi on the carbon cloth was about 0.5mg cm^{-2}. The PANi/Carbon cloth of each piece was weighted and averaged several times to calculate the mass loading of PANi.

2.5 Material Characterization

2.5.1Tensile testing

Hydrogels were cut into 2mm wide strips for tensile testing. The thickness of. each sample was measured with a caliper. For the low temperature tensile testing, samples were stored in freezer (-20℃) for 2 hours, then quickly took out to do the tensile test. The data were obtained using a Cellscale Univert mechanical tester with a 50N loading cell installed.

2.5.2 Compression testing

Hydrogels were cut into 2mm x 2mm square piece for compression testing. The. thickness of each sample was measured with a caliper. For the low temperature compression testing, samples were stored in freezer (-20℃) for 2 hours, then quickly took out to do the compression test. The data were obtained using a Cellscale Univert mechanical tester with a 50N loading cell installed.

2.5.3 SEM Characterizations

All hydrogel samples were immersed in pure water for 24 h to remove the salts. Then the samples were frozen in liquid nitrogen and freeze-dried using the Labconco FreeZone freeze drier. To characterize dendrite growth, the Zn anodes were taken out from the battery and washed with water. The freeze-dried hydrogels and Zn anodes were sputtered with gold and observed using a ZEISS Supra 40VP SEM.

2.5.4 XRD characterization

The Zn anodes were taken out from the battery and washed with water. XRD. was recorded on a 18 kW rotating target X-ray diffractometer (MAX-2550VB).

2.5.5 DSC characterization

Hydrogels treated with DMSO-containing hybrid solutions with different. DMSO/H_2O ratios were characterized using a differential scanning calorimeter

(DSC-Q8000). Hydrogel samples were sealed in aluminum pans for testing, with an empty pan used as the reference. Samples were equilibrated at 20 °C and then cooled to −70 °C.

2.5.6 Raman spectroscopy characterization

Hydrogels treated with $ZnSO_4$ solutions with different DMSO/H_2O weight. ratios and pure DMSO were characterized using a Raman spectroscopy (RENISHAW inVia Raman Microscope, Model: HeNe). All the samples were tested under the setup of 633nm laser wavelength, x5 of the magnification of the optical microscope, 10 seconds exposure time, 50% laser power, and 5 times accumulations.

3 Results and discussions

3.1 Fabrication of gel electrolytes

The fabrication procedure of the hydrogel electrolyte is shown in Figure 1a. 10wt% PVA-DMSO solution was mixed with a 10wt% PVA-H_2O solution at a 3:2 weight ratio. Then, the mixture was degassed and poured into molds for gelation. During the gelation process, both the DMSO and water would significantly interact with PVA, facilitating the hydrogen bonding formation between the polymer chains and producing crystallites as physical crosslinking sites for the hydrogel (Figure 1a, 1b) [17]. After one hour of gelation, the translucent hydrogels were immersed in a DMSO/H_2O/$ZnSO_4$ solution for 96 hours to form the gel electrolytes. The obtained product are named in the order of their liquid phase DMSO contents (Table S1) .

	DMSO (g)	H_2O (g)	$ZnSO_4 \cdot 7H_2O$ (g)
PVA-X_0	0	500	287.56
PVA-X_{10}	50	450	287.56
PVA-X_{20}	100	400	287.56
PVA-X_{30}	150	350	287.56
PVA-X_{40}	200	300	287.56
PVA-X_{50}	250	250	287.56
PVA-X_{60}	300	200	287.56

Table 1. Component of the soaking solution for each PVA hydrogel electrolytes

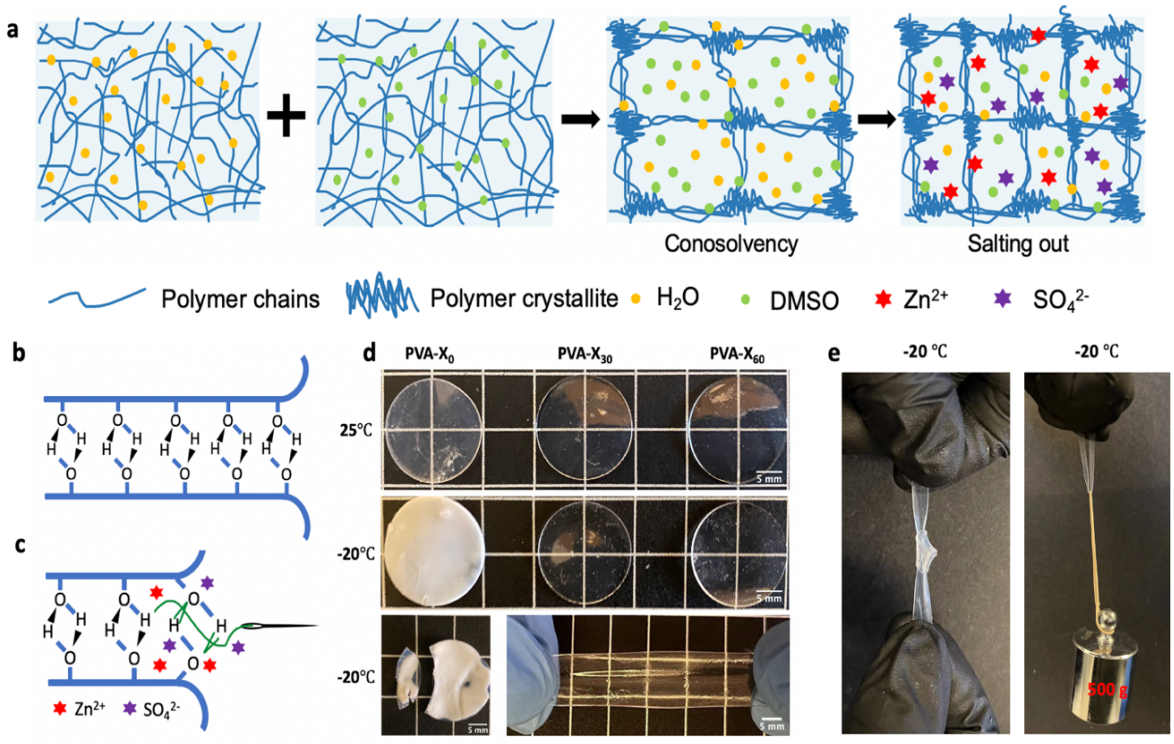

Figure 1. (a) The fabrication process of the hydrogels. **(b)** The hydrogen bond interaction among the PVA polymer chains. **(c)** The interaction among ions and polymer chains. The Zn^{2+} and SO_4^{2-} ions promote the formation of new hydrogen bonds between the hydroxyl groups forming the aggregation/crystallization of PVA. **(d)** Photographs of PVA-X_0, PVA-X_{30}, and PVA-X_{60} at 25℃ and -20℃, after salting out for 96 hours. At -20℃, PVA-X_0 became opaque and brittle, it can be easily breaking into two parts when we stretch it. In contrast, PVA-X_{30} and PVA-X_{60} remain translucent and flexible, and can still be stretched as shown in the bottom right corner. **(e)** Photographs of knotting PVA-X_{30} and using it to hold 500g weight at -20℃.

3.2 Characterization of gel electrolytes

In order to validate the hydrogels can serve as tough and anti-freezing electrolytes, their morphologies, ionic conductivities, stress-strain behaviors, and freezing temperatures

were investigated. The ionic conductivity of hydrogels is shown in Figure 2, which is calculated from the Nyquist plots (Figure 2). At 25℃, the PVA-X_0 has the highest ionic conductivity (25mS/cm).

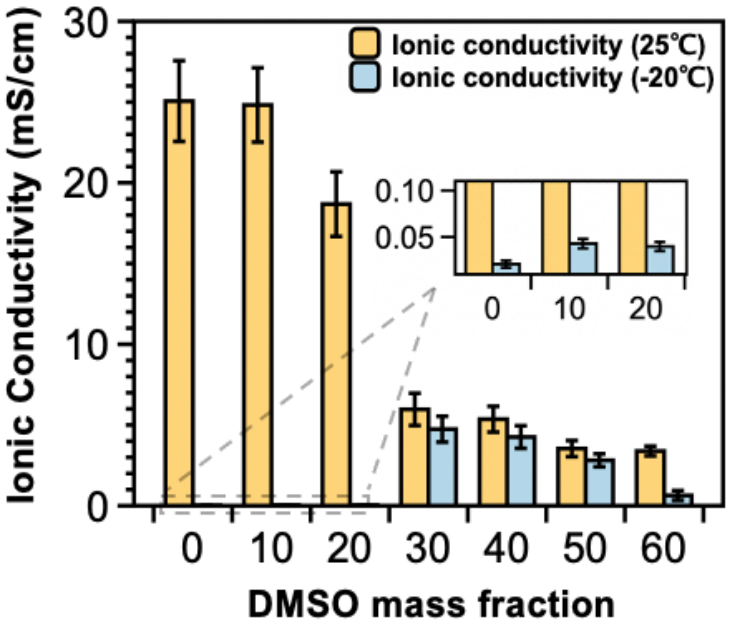

Figure 2. Ionic conductivities of different hydrogel samples tested at 25 ℃ and -20 ℃.

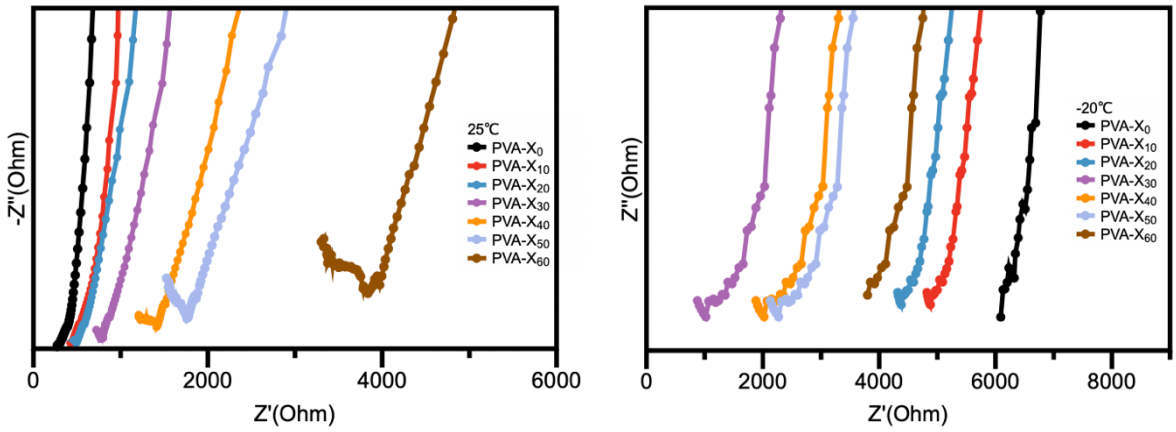

Figure 3. Nyquist plot of PVA-X_0, PVA-X_{10}, PVA-X_{20}, PVA-X_{30}, PVA-X_{40}, PVA-X_{50}, and PVA-X_{60} at 25℃ and -20℃.

However, the ionic conductivity of PVA-X_0, PVA-X_{10}, and PVA-X_{20} are extremely low due to the freezing of the liquid content inside the hydrogels at -20℃. The highest ionic conductivity at -20℃ was 5.971 mS/cm from PVA-X_{30}, and it decreased with the increasing DMSO content, which might resulted from the larger pore size of the PVA-X_{30} (Figure 4), and the decrease of ion mobility due to the increase of the size of the zinc ion complexes inside the solution when the DMSO content increased [16].

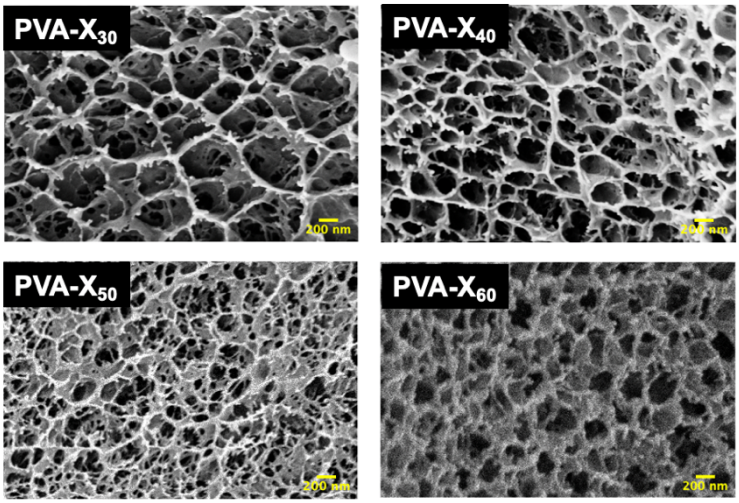

Figure 4. SEM images of PVA-X_{30}, PVA-X_{40}, PVA-X_{50}, and PVA-X_{60}.

To study the specific ion effect on PVA, various zinc salts which are able to dissolved in the DMSO/H_2O solution were tested, including zinc acetate ($ZnAc_2$), zinc chloride ($ZnCl_2$), zinc perchlorate ($Zn(ClO_4)_2$), and $ZnSO_4$.

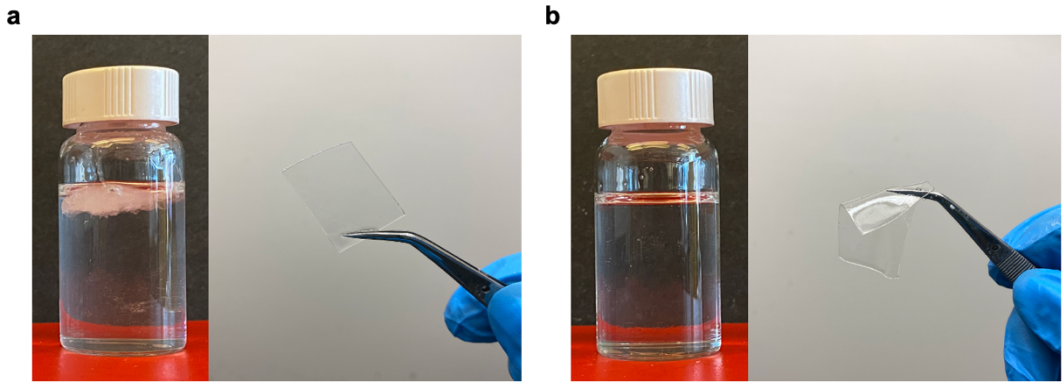

Figure 5. a) PVA salting-out in the $ZnSO_4$, b) PVA salting-in in $ZnAc_2$, $ZnCl_2$, and $Zn(ClO_4)_2$.

As shown in Figure 5, PVA in the 2M $ZnSO_4$/DMSO/H_2O solution became white and opaque clumps, showing ZnSO4 have "salting-out" effect on PVA, which can enhance the mechanical property of the PVA hydrogels. In contrast, the PVA dispersed in the 1M $ZnAc_2$, 1M $ZnCl_2$, and 1M $Zn(ClO_4)_2$ /DMSO/H_2O solutions, showing their "salting-in" effect, which enhance the solubility of the polymer chain and degrade the robustness of the PVA hydrogel [17].

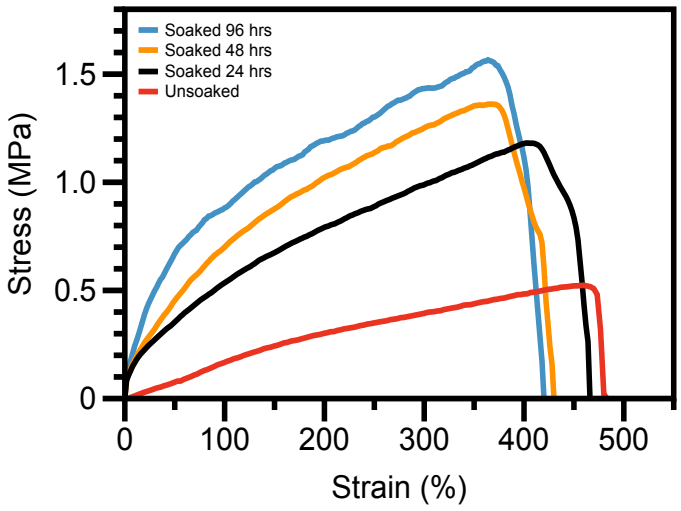

Figure 6. Stress-strain curves of conosolvency polyvinyl alcohol (PVA) hydrogels before and after soaked in 2M $ZnSO_4$-X_{30} electrolyte for 24, 48, and 96h.

The effect of soaking time to the mechanical properties is also investigated. Before soaking into the DMSO-containing hybrid solutions, the conosolvency PVA hydrogels ultimate tensile strength and toughness are 0.4MPa and 1.2MJ/m^3 (Figure 6). After the 96hr soaking process, the polymer chains have enough time to aggregate and form the crystalline domains, thus the ultimate tensile strength and toughness increase to 2.8MPa and 8.75MJ/m^3, 1.9MPa and 5.7MJ/m^3, 1.8MPa and 6.1MJ/m^3, 1.5MPa and 4.56MJ/m^3, 1.7MPa and 4.74MJ/m^3, 1.86MPa and 6.34MJ/m^3, 2.1MPa and 6.73MJ/m^3 for PVA-X_0 to PVA-X_{60}, respectively (Figure 7).

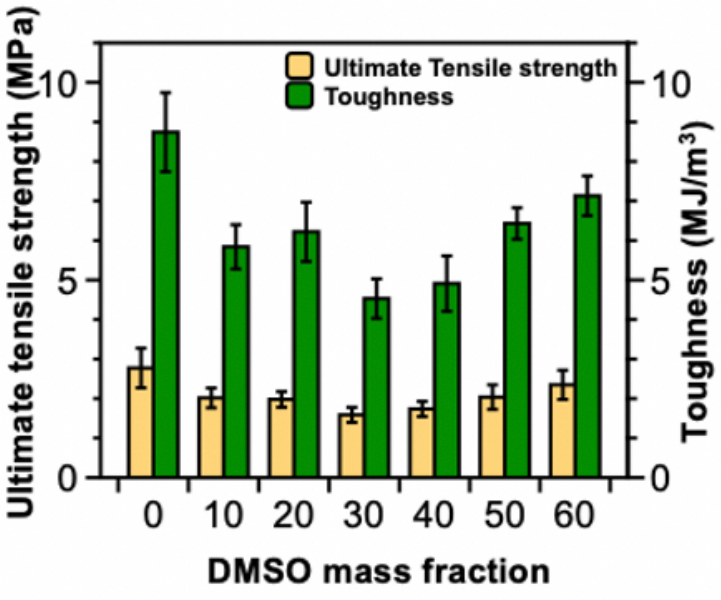

Figure 7. Ultimate tensile strength and toughness of different hydrogel samples.

As shown, the PVA-X_0 and PVA-X_{60} were stronger than PVA-X_{30}, which can be explained from the smaller pore size (Figure 8) and more fiber-like structures (Figure 9).

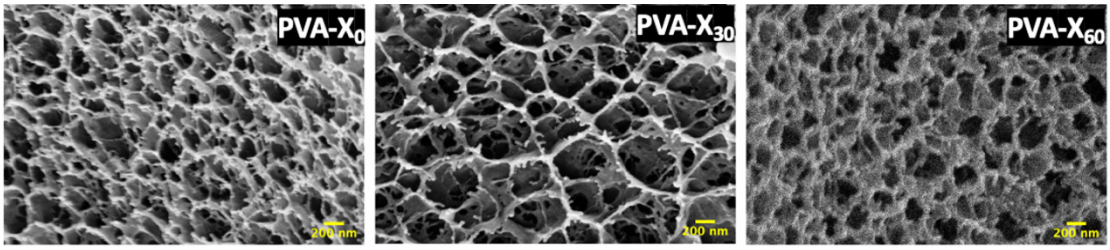

Figure 8. SEM images of PVA-X_0, PVA-X_{30}, and PVA-X_{60}.

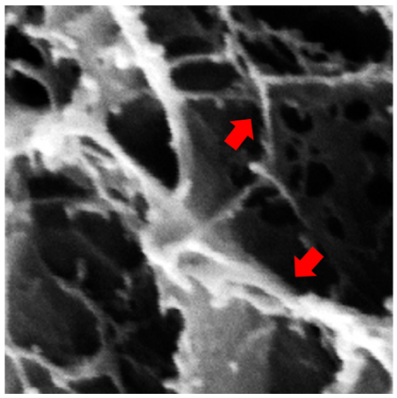

Figure 9. SEM image of the fiber structure inside the PVA hydrogels electrolytes

Despite the PVA-X_{30} not being as strong as the other recipes, it was still much stronger than the commonly used commercial glass fiber separator (Figure 3f), showing 5 times and 300 times higher ultimate tensile strength and toughness. Additionally, the mechanical strength outperformed previous research as shown in Table 2 [10][18][19][20][21][22][23].

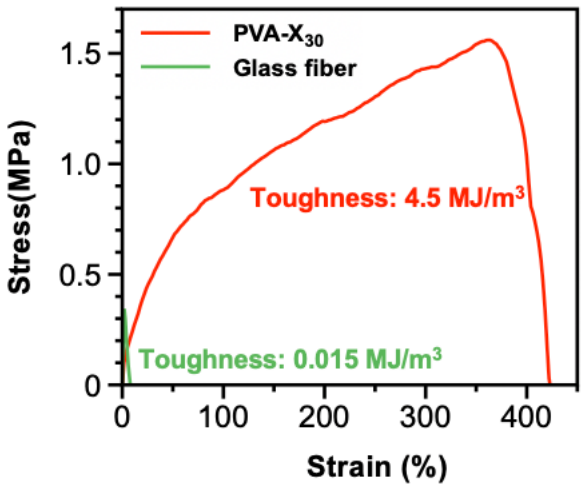

Figure 10. Stress-strain curves of PVA-X_{30} and commercial glass fiber. The toughness of PVA-X_{30} is 300 times larger than the commercial glass fiber.

	This work	[10]	[15]	[19]	[20]	[21]	[22]	[23]
Hydrogel electrolyte type	PVA, DMSO, $ZnSO_4$	Polyacrylamide (PAAm), Lithium Chloride (LiCl), $ZnSO_4$,	PVA + Glycerol + Borax, $ZnSO_4$, Manganese sulfate ($MnSO_4$),	Elastomer coated PAAM + Alginate, $ZnSO_4$, $MnSO_4$, Ethylene glycol	Xanthan gum, $ZnCl_2$	Polyacrylic acid (PAAc) + Sodium hydroxide (NaOH), Potassium hydroxide (KOH)	Methyl Cellulose + Polyelectrolyte poly(2-acrylamido-2-methylpropanesulfonic acid (PAMPs), KOH	PAAc + PAAm, KOH, $Zn(Ac)_2$, glycerol
Ultimate tensile strength (MPa)	1.585	0.085	0.12	0.048	>0.1	0.083	0.057	0.145

Table 2. Mechanical property of this work and other anti-freezing hydrogels type

For practical applications, the gel electrolytes need to exhibit good mechanical strength even at subzero temperature. As shown in Figure 1d, at -20℃ both the PVA-X_{30} and PVA-X_{60} remain transparent and flexible, while the PVA-X_0 becomes opaque and brittle. Moreover, PVA- X_{30} and PVA-X_{60} can be knotted and is able to hold a 500 g weight at -20 ℃ (Figure 1e). To further demonstrate the anti-freezing property of hydrogels, tensile and compression tests were conducted at 25 °C, 0 °C, and - 20 °C. As shown in Figure 11a, the Young's modulus increases with the decreasing temperature, while there was little change in the elongation at break. The same modulus trend can also be found in the compression test (Figure 11b), which shows the excellent anti-freezing property of the hydrogel.

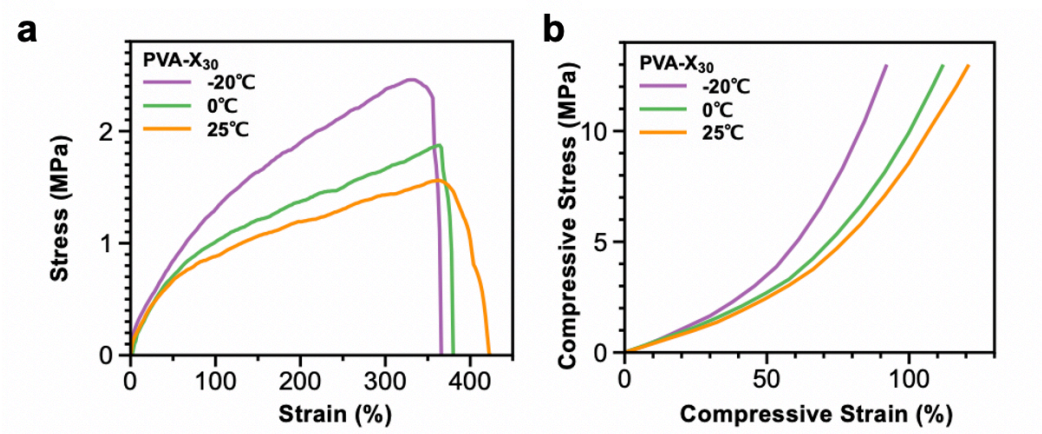

Figure 11. (a) Tensile stress-strain curves of PVA-X_{30} at 25 ℃, 0 ℃, and -20 ℃. (b) Compressive stress-strain curves of PVA-X_{30} at 25 ℃, 0 ℃, and -20 ℃.

The freezing temperatures of the hydrogels were measured with a differential scanning calorimeter (DSC) (Figure 12). As shown, no peak was observed for the PVA-X_{30} and PVA-X_{60} when the testing temperature drops to -20 ℃, demonstrating that the phase transition temperature is lower than -20 ℃. This is due to the strong interaction between the DMSO and water molecules which prevent the water-water interaction.

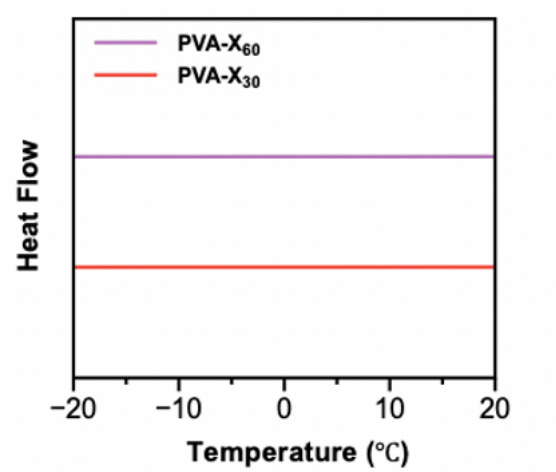

Figure 12. DSC curves of PVA-X_{30}, and PVA-X_{60}.

Raman spectroscopy was applied to further prove the anti-freezing property of the hydrogel. Figure 13 showed the Raman spectra of pure DMSO, PVA-X_0, PVA-X_{30} and PVA-X_{60}. The shifting of the S=O and CH_3 band with increasing DMSO concentration proves that water molecules could be attracted by the DMSO, and sturdy S=O··H-O hydrogen bonds could be formed among these two, highly regulating the free water molecules inside the solution and decreasing the freezing temperature [16].

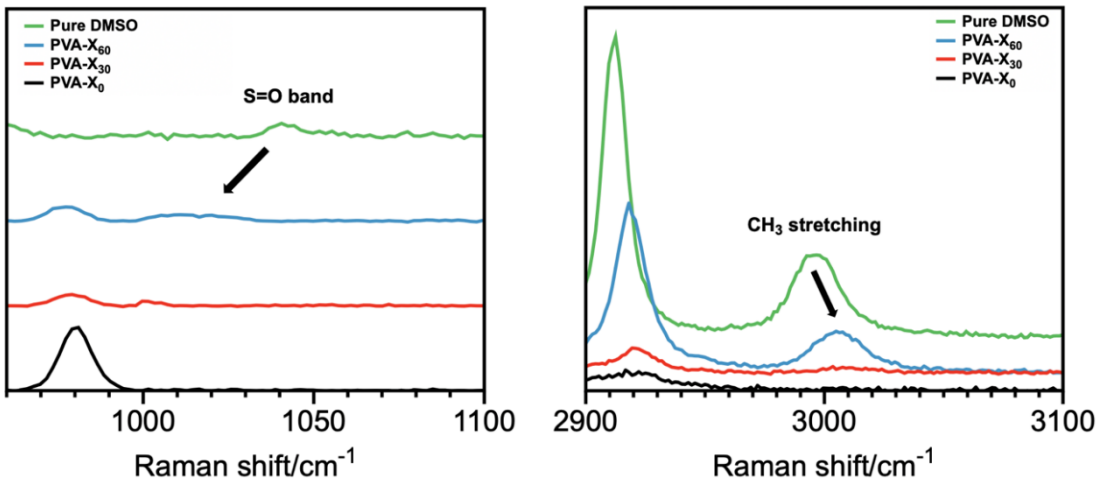

Figure 13. Raman spectra of the Pure DMSO and PVA gel electrolyte

3.3 Electrochemical performances

The hydrogels were deployed in Zn/Zn or Zn/PANi cells to showcase their ability as anti-freezing zinc-ion battery electrolytes. Zn/Zn cells were evaluated at room temperature with an areal capacity of 1mAh/cm^2, as shown in Figure 14. The voltage curve of the cells using PVA-X_{30} and PVA-X_{60} can retain their shapes for over 300 h and 230 h without any significant fluctuation, respectively. However, the cells with PVA-X_0 was only stable for 60 h before shorting due to the dendrite formation [16][18][19][26].

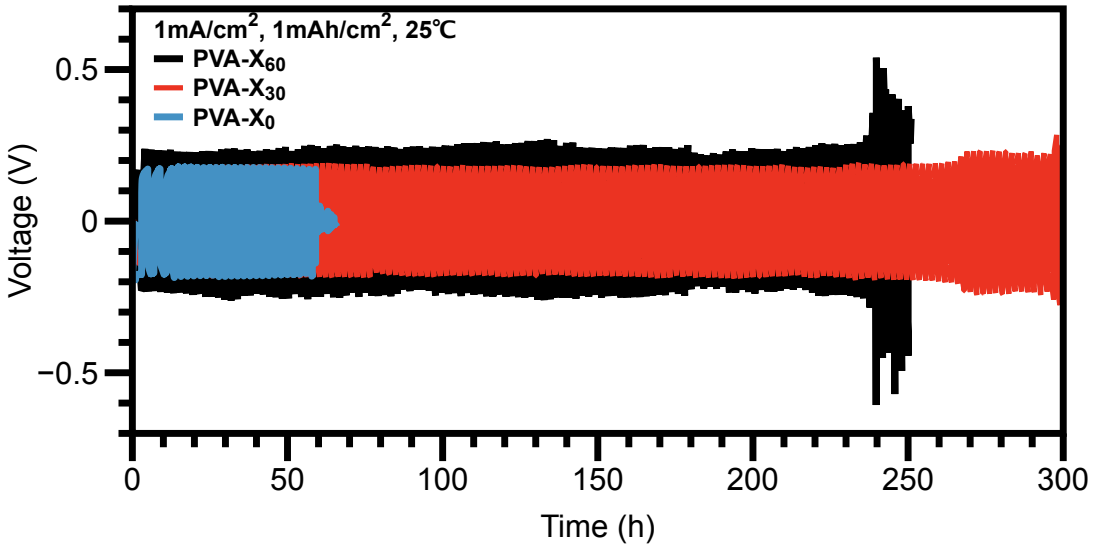

Figure 14. The galvanostatic charge/discharge (GCD) curves of the Zn/Zn symmetric batteries with PVA-X_0, PVA-X_{30}, and PVA-X_{60} at 1mA/cm^2, 1mAh/cm^2 and 25℃.

SEM images of the Zn foils in Zn||Zn cells after 50 cycles (1mA/cm^2, 1mAh/cm^2, under RT) were collected to demonstrate the dendrite suppression. As shown, the Zn metal surface with PVA-X_0 in Zn/Zn cells was covered with a large number of sharp dendrites, comprised of several zinc hexagonal plates grown over each other in perpendicular direction. Whereas, for the PVA-X_{30} and PVA-X_{60}, the zinc hexagonal plates tend to grow in parallel direction over the Zn metal surface (Figure 15).

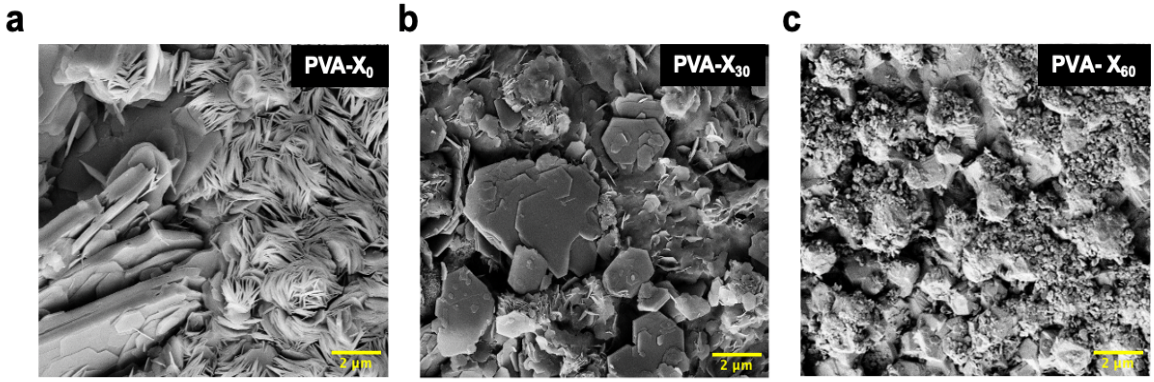

Figure 15. Surfaces SEM images of the Zn foils in Zn/Zn batteries after 50 cycles at 1mA/cm^2, 1mAh/cm^2 with **(a)** PVA-X_0, **(b)** PVA-X_{30}, **(c)** PVA-X_{60}.

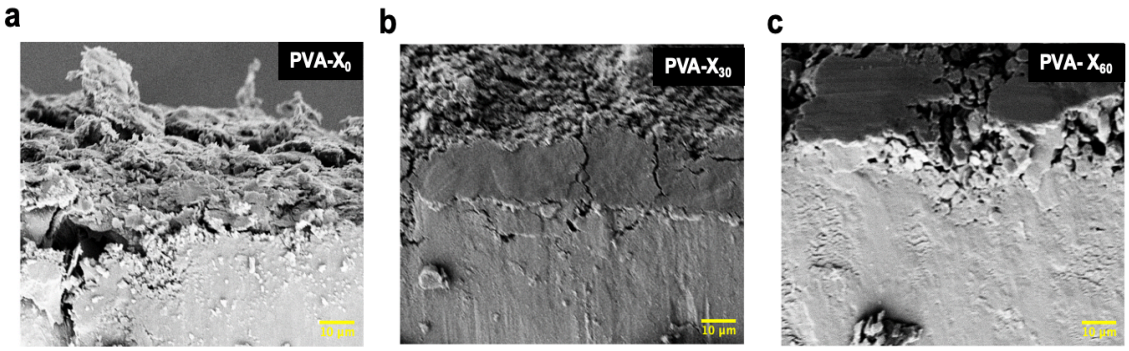

Figure 16. Cross-sectional SEM images of the Zn foils in Zn/Zn batteries after 50 cycles at 1mA/cm^2, 1mAh/cm^2 with **(a)** PVA-X_0, **(b)** PVA-X_{30}, **(c)** PVA-X_{60}.

Figure 16 shows the cross-sectional views of the Zn metal surface. Obviously, the PVA-X_0 sample's Zn metal surface is rough and several dendrites are formed over the surface, yet both the PVA-X_{30} and PVA-X_{60}'s Zn metal surface remain flat and homogeneous. SEM images of Zn foils after 200 cycles with PVA-X_{30} and PVA-X_{60} were also provided and no sharp dendrites were observed (Figure 17).

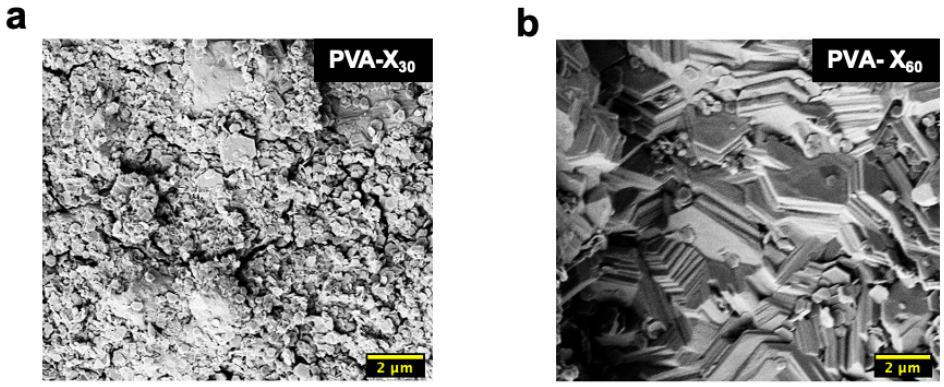

Figure 17. Surfaces SEM images of the Zn foils in Zn/Zn batteries after 200 cycles at 1mA/cm^2, 1mAh/cm^2 with **(a)** PVA-X_{30} and **(b)** PVA-X_{60}.

X-ray diffraction (XRD) was employed to evaluate the products of the Zn plating with different hydrogel samples after 50 cycles. As exhibited in Figure 18, the peak at 2theta = 36.5°, corresponding to the (002) plane, became stronger when the DMSO concentration increased, which indicates that DMSO can promote the homogeneous Zn deposition on (002) direction and restrain dendrite growth and lead to longer battery

cycling life. While PVA-X_{60} is most effective in inducing (002) growth, its small pore sizes hinders the mass transport and leads to the occurrence of voltage polarization. Therefore, PVA-X_{30} was chosen for additional characterization because of its achieve balanced performance between dendrite resistance and mass transport.

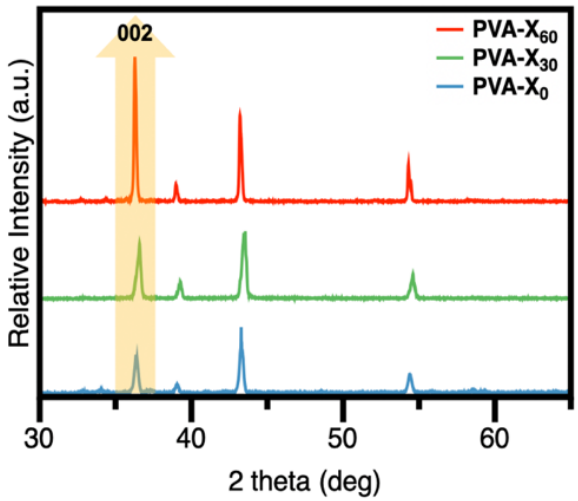

Figure 18. XRD patterns of the Zn foils in Zn/Zn batteries after 50 cycles at 1mA/cm^2, 1mAh/cm^2 with **(a)** PVA-X_0, **(b)** PVA-X_{30}, **(c)** PVA-X_{60}.

Zn/Zn cells with PVA-X_{30} were tested at 3mA/cm^2, 3mAh/cm^2 and 25 C, also at 0.5mA/cm^2, 1mAh/cm^2 and -20℃. As shown in Figure 19, these cells can remain stable for at least 120hr at high current density and high capacity at room temperature, and able to work at -20℃ for at least 200hr, showcasing the stability and freezing tolerance of the PVA-X_{30} electrolyte.

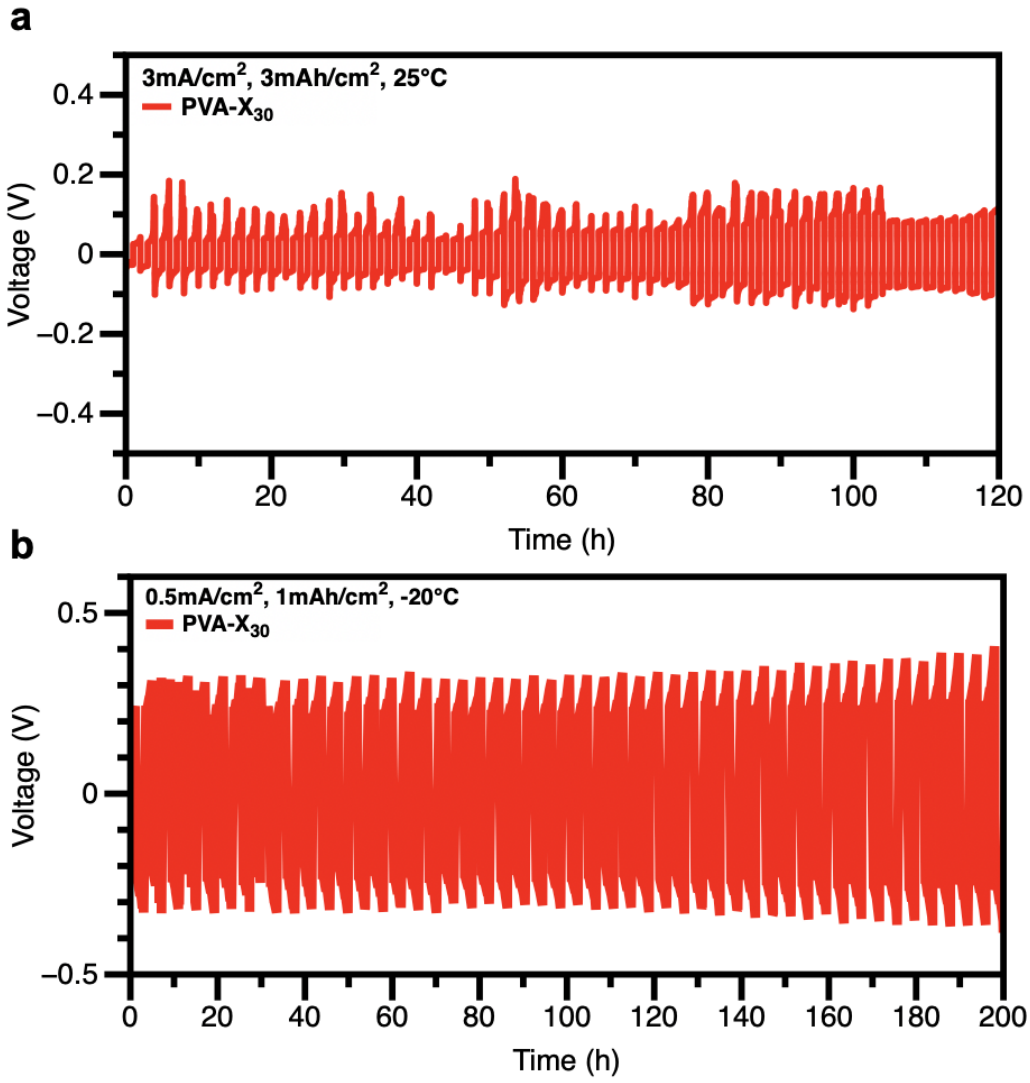

Figure 19. GCD curves of the Zn/Zn symmetric batteries with PVA-X_{30} at **(a)** 3mA/cm², 3mAh/cm² and 25℃, **(b)** 0.5mA/cm², 1mAh/cm² and -20℃

Zn/polyaniline (PANi) full batteries (Figure 20a) were tested to show the practical application of PVA-X_{30}. PANi was chosen as the cathode, owing to its high conductivity and inherent elasticity, and the SEM images of the as prepared PANi cathode are shown in Figure 21 [28][29][30]. The rate performance of the full batteries at 25℃ and -20℃

are shown in Figure 20b, 20c. The battery could provide a high reversible capacity of 90 mAh/g at a current density of 5A/g at RT. At -20°C, the battery displayed capacity as high as 87 mAh/g at 0.1A/g, and could maintain that same value even after cycling at higher current densities; this indicates that the low capacity at higher current density is mainly due to the kinetic of ion transport instead of the structural degradation of PVA-X_{30}.

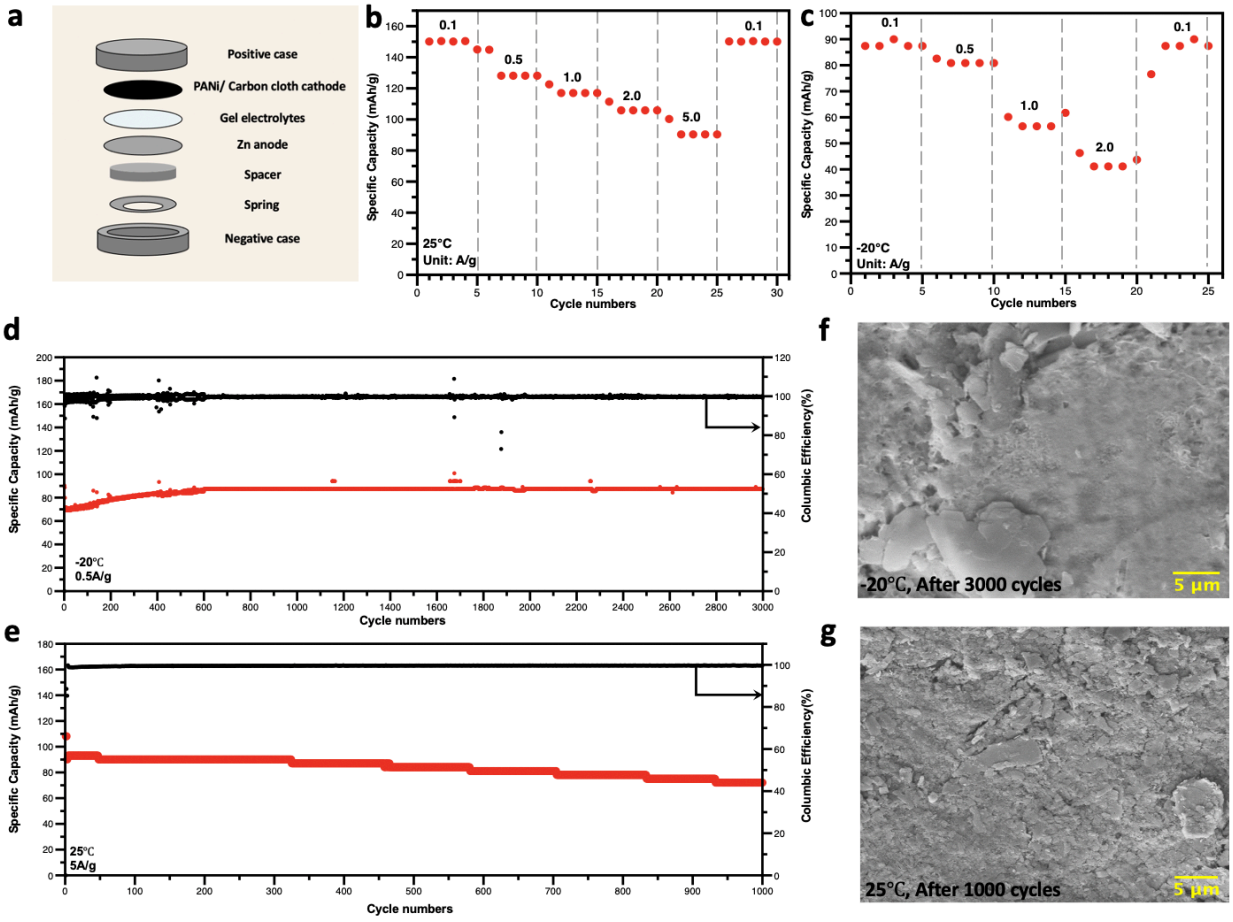

Figure 20. (a) Schematics of the Zn/PANi full batteries. Rate performances of the batteries with PVA- X_{30} at **(b)** 25°C and **(c)** -20°C. Cycling performance of the batteries at **(d)** -20°C and **(e)** 25°C. SEM images of the Zn anode in the Zn/PANi

batteries after cycling at **(f)** -20℃ and **(g)** 25℃.

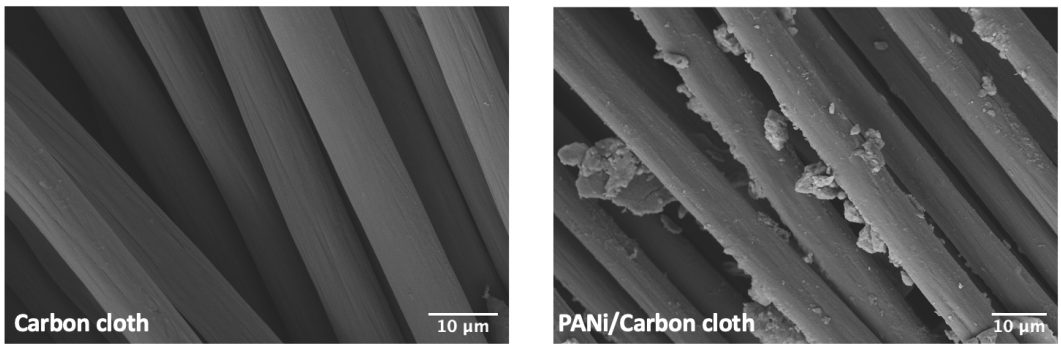

Figure 21. SEM images of Carbon cloth and PANi/Carbon cloth. Showing that PANi has been successfully grown over the carbon cloth.

The cyclability of the Zn/PANi batteries with PVA-X_{30} was evaluated at 0.5A/g under -20℃ and 5A/g under RT, as shown in Figure 20d, 20e. At 25℃, our battery exhibited a high capacity of 78mAh/g after 1000 cycles and the corresponding Columbic efficiency remained almost 100%. At -20℃, the capacity remained 83 mAh/g after 3000 cycles with almost 100 % columbic efficiency. The charge/discharge curves are shown in Figure 22. These excellent electrochemical performances can be attributed to the dendrite-suppressing properties of the DMSO. From Figure 20f, 20g, it was shown that after 1000 cycles at room temperature and 3000 cycles tests at -20℃, the surfaces of the Zn metal were observed to remain smooth and lacked perpendicular zinc crystal dendrites.

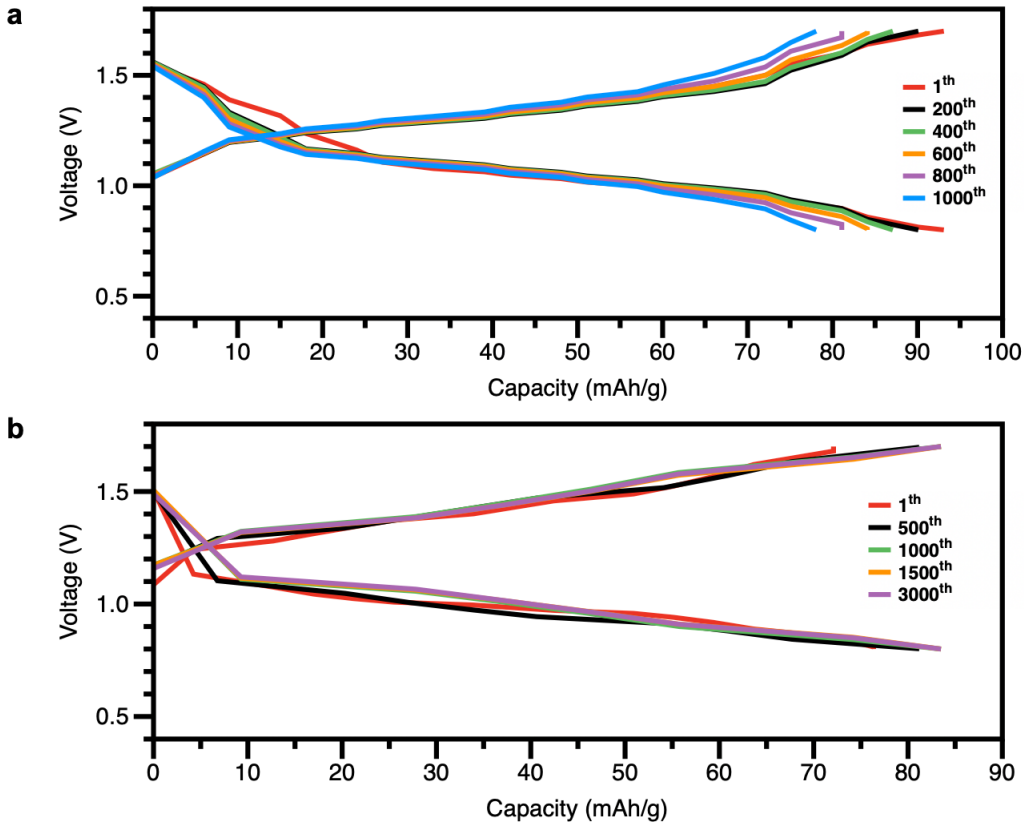

Figure 22. The charge/discharge curves of the Zn/PANi batteries with PVA-X_{30} at **(a)** 5A/g and 25℃, **(b)** 0.5A/g and -20℃.

To further verify the electrochemical performance of our Zn/PANi battery with PVA-X_{30} under mechanical deformation or impact, a soft-pack battery was assembled (Figure 23a). Cyclic voltammetry curves showed peaks at 1.35V and 0.95V vs Zn/Zn^{2+} corresponding to the storage/release of ions from the PANi [31][32] (Figure 23b). Figure 23c demonstrated that the battery possesses the anti-freezing property and was tough enough to endure the hammering while still being able to light up the LED bulb. Low temperature bending tests were conducted to show the flexibility and anti-freezing

property of our PVA-X_{30} Zn/PANi battery. As shown in Figure 23d, the PVA-X_{30} battery was first tested in the unbent state for 5 cycles, then it was bent during the subsequent 5 cycles; each state was tested 3 times inside the refrigerator. The capacity of the battery was tested under 0.5A/g current density: the PVA-X_{30} battery's capacity remained ~75 mAh/g after 30 cycles. This test showed that our hydrogel electrolytes can offer outstanding mechanical property and durability in practical situations.

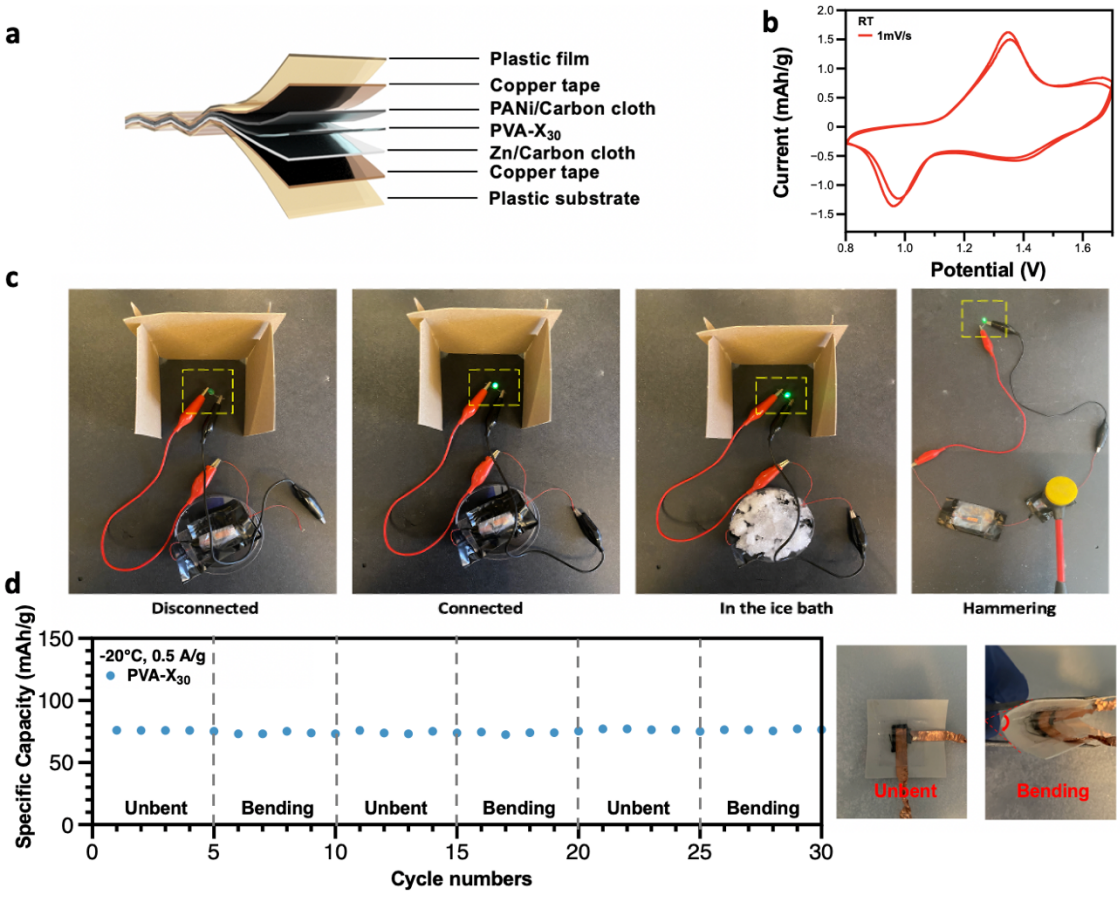

Figure 23. **(a)** Schematics of the soft-pack Zn/PANi battery with PVA-X_{30}. **(b)** The CV curves of the battery at 1mV/s under RT. **(c)** Demonstration of the Zn/PANi battery with PVA-X_{30} is able to light up the LED, even after being soaked in the ice bath or

hammered. **(d)** Capacity evolution of the Zn/PANi battery with PVA-X_{30} and Zn/PANi battery with Glass Fiber-X_{30} at 0.5A/g and -20℃.

Furthermore, in order to show better practicability than the commercial glass-fiber, soft-pack battery hitting tests were conducted. The test setup of Zn/PANi with a commercial glass-fiber and with a PVA-X_{30} is shown in Figure 24. As shown, after 1 times of hitting, the former one can no longer light up the LED bulb; however, the latter one can still work even after 10 hits. Figure 25 exhibited the appearance of these two batteries after the hitting test. The commercial glass-fiber got smashed, which caused shorting. In contrast, no apparent damage is found on the PVA-X_{30}, proving that it is more suitable to be applied practically.

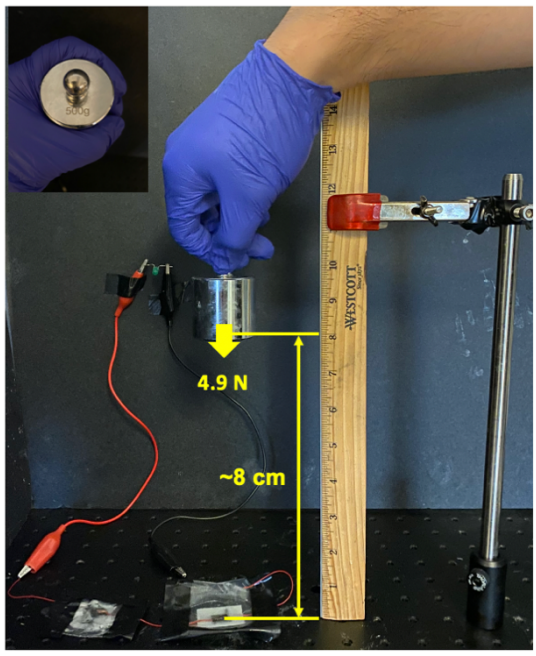

Figure 24. The demonstration of the battery hitting test. Weight (500g) was hold at 8cm above the ground.

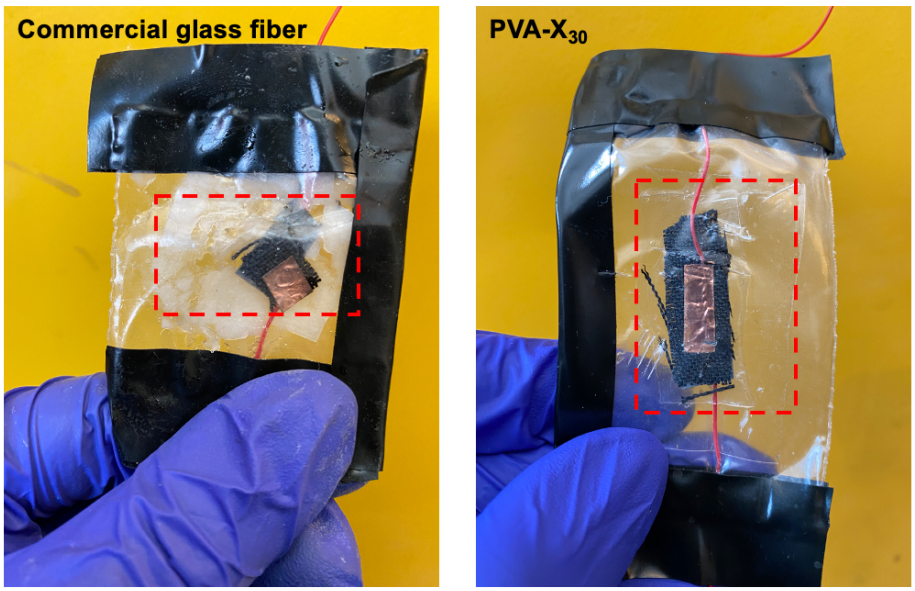

Figure 25. Appearance of the Zn/PANi batteries with PVA-X_{30} and commercial glass fiber after the hitting test.

The strength of the hydrogel electrolyte could be increased further by tuning the molecular weight (Mw) of the PVA. By increasing the Mw from 89 kDa to 195kDa, the toughness of the hydrogel could be increased about six-fold. The hydrogel was strong enough to hold a five-gallon bottle of water (Figure 26a,b).

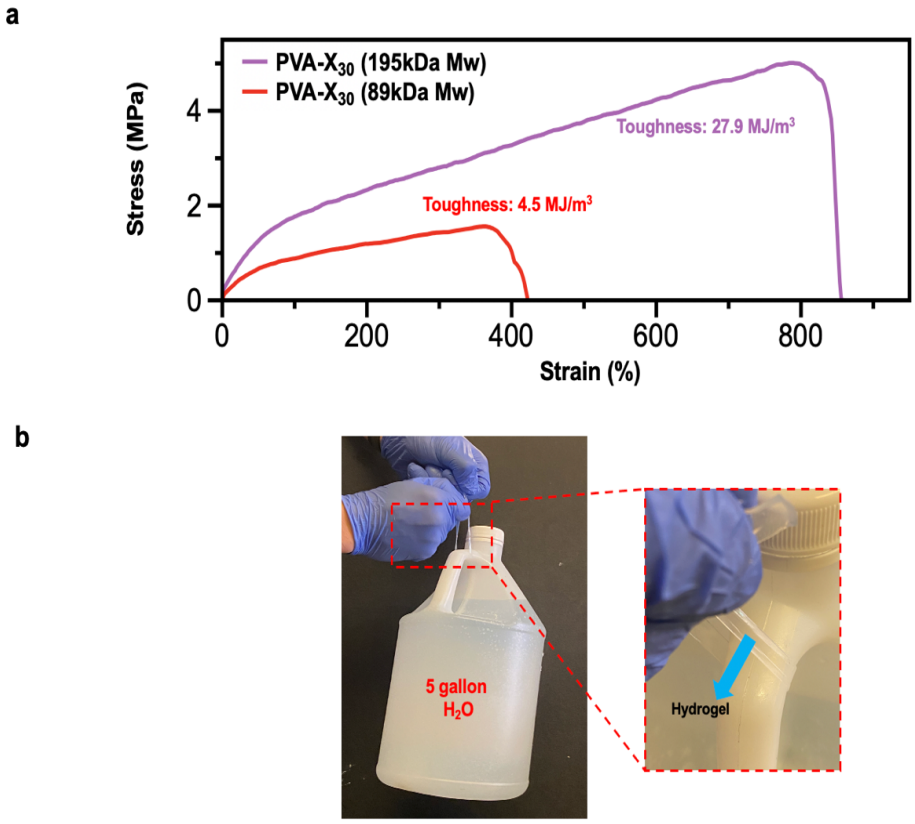

Figure 26. (a) Stress-Strain curve of PVA-X_{30} with different Mw. The toughness can be increased 6 times through increasing the Mw of PVA from 89kDa to 195kDa. **(b)** Demonstration of the high toughness of 195kDa Mw PVA- X_{30}, which is able to hold a 5-gallon water bottle.

4 Conclusion

Hydrogel electrolyte research has greatly increased due to the growing pursuit of flexible electronics. In this study, an anti-freezing, dendrite-suppressing, and tough hydrogel electrolyte was developed through utilizing a $ZnSO_4$/DMSO/H_2O electrolyte in PVA. The hydrogel showed good mechanical properties, with a tensile strength of 1.5MPa and a toughness of 4.5MJ/m^3. The electrolyte also offered a high ionic conductivity of 4.743 mS/cm at -20 ℃ and a dendrite-suppressing performance, enabling stable and reversible battery operation in a Zn/PANi cell. At 25℃, the capacity remained at 78mAh/g after 1000 cycles when subjected to 5A/g; meanwhile at -20℃, the capacity could be maintained at 83mAh/g after 3000 cycles at 0.5A/g. In addition, the soft-pack battery made with PVA-X_{30} showed outstanding durability and stability at -20℃. The capacity of our flexible battery can remain nearly unchanged despite being bent at low temperature, showing its potential in harsh environments. We anticipate that the proposed method will further expand the range of hydrogel electrolyte applications for emerging flexible power supplies.

5 References

[1] M. Armand, “Nature Lithium Battery,” *Nature*, vol. 414, no. November, pp. 359–367, 2001, [Online]. Available: http://www.ncbi.nlm.nih.gov/pubmed/11713543.

[2] P. Yu, Y. Zeng, H. Zhang, M. Yu, Y. Tong, and X. Lu, “Flexible Zn-Ion Batteries: Recent Progresses and Challenges,” *Small*, vol. 15, no. 7, 2019, doi: 10.1002/smll.201804760.

[3] N. Zhang, X. Chen, M. Yu, Z. Niu, F. Cheng, and J. Chen, “Materials chemistry for rechargeable zinc-ion batteries,” *Chem. Soc. Rev.*, vol. 49, no. 13, pp. 4203–4219, 2020, doi: 10.1039/c9cs00349e.

[4] X. Jia, C. Liu, Z. G. Neale, J. Yang, and G. Cao, “Active Materials for Aqueous Zinc Ion Batteries: Synthesis, Crystal Structure, Morphology, and Electrochemistry,” *Chem. Rev.*, vol. 120, no. 15, pp. 7795–7866, 2020, doi: 10.1021/acs.chemrev.9b00628.

[5] L. E. Blanc, D. Kundu, and L. F. Nazar, “Scientific Challenges for the Implementation of Zn-Ion Batteries,” *Joule*, vol. 4, no. 4, pp. 771–799, 2020, doi: 10.1016/j.joule.2020.03.002.

[6] S. Huang, F. Wan, S. Bi, J. Zhu, Z. Niu, and J. Chen, “A Self-Healing Integrated All-in-One Zinc-Ion Battery,” *Angew. Chemie - Int. Ed.*, vol. 58, no.

13, pp. 4313–4317, 2019, doi: 10.1002/anie.201814653.

[7] B. Tang, L. Shan, S. Liang, and J. Zhou, “Issues and opportunities facing aqueous zinc-ion batteries,” *Energy Environ. Sci.*, vol. 12, no. 11, pp. 3288–3304, 2019, doi: 10.1039/c9ee02526j.

[8] L. Cao *et al.*, “Highly Reversible Aqueous Zinc Batteries enabled by Zincophilic–Zincophobic Interfacial Layers and Interrupted Hydrogen-Bond Electrolytes,” *Angew. Chemie - Int. Ed.*, vol. 60, no. 34, pp. 18845–18851, 2021, doi: 10.1002/anie.202107378.

[9] Q. Zhang *et al.*, “Modulating electrolyte structure for ultralow temperature aqueous zinc batteries,” *Nat. Commun.*, vol. 11, no. 1, pp. 1–10, 2020, doi: 10.1038/s41467-020-18284-0.

[10] M. Zhu *et al.*, “Antifreezing Hydrogel with High Zinc Reversibility for Flexible and Durable Aqueous Batteries by Cooperative Hydrated Cations,” *Adv. Funct. Mater.*, vol. 30, no. 6, pp. 1–10, 2020, doi: 10.1002/adfm.201907218.

[11] N. Chang *et al.*, “An aqueous hybrid electrolyte for low-temperature zinc-based energy storage devices,” *Energy Environ. Sci.*, vol. 13, no. 10, pp. 3527–3535, 2020, doi: 10.1039/d0ee01538e.

[12] M. Chen, J. Chen, W. Zhou, X. Han, Y. Yao, and C. P. Wong, “Realizing an All-

Round Hydrogel Electrolyte toward Environmentally Adaptive Dendrite-Free Aqueous Zn–MnO2 Batteries," *Adv. Mater.*, vol. 33, no. 9, 2021, doi: 10.1002/adma.202007559.

[13] J. Liu, Z. Khanam, S. Ahmed, T. Wang, H. Wang, and S. Song, "Flexible Antifreeze Zn-Ion Hybrid Supercapacitor Based on Gel Electrolyte with Graphene Electrodes," *ACS Appl. Mater. Interfaces*, vol. 13, no. 14, pp. 16454–16468, 2021, doi: 10.1021/acsami.1c02242.

[14] Y. Zhao *et al.*, "Aqueous Rechargeable Metal-Ion Batteries Working at Subzero Temperatures," *Adv. Sci.*, vol. 8, no. 1, pp. 1–13, 2021, doi: 10.1002/advs.202002590.

[15] M. Chen *et al.*, "Anti-freezing flexible aqueous Zn-MnO2 batteries working at -35 °c enabled by a borax-crosslinked polyvinyl alcohol/glycerol gel electrolyte," *J. Mater. Chem. A*, vol. 8, no. 14, pp. 6828–6841, 2020, doi: 10.1039/d0ta01553a.

[16] D. Feng, F. Cao, L. Hou, T. Li, Y. Jiao, and P. Wu, "Immunizing Aqueous Zn Batteries against Dendrite Formation and Side Reactions at Various Temperatures via Electrolyte Additives," *Small*, vol. 17, no. 42, 2021, doi: 10.1002/smll.202103195.

[17] S. Wu *et al.*, "Poly(vinyl alcohol) Hydrogels with Broad-Range Tunable

Mechanical Properties via the Hofmeister Effect," *Adv. Mater.*, vol. 33, no. 11, 2021, doi: 10.1002/adma.202007829.

[18] S. Wu *et al.*, "Rapid and scalable fabrication of ultra-stretchable, anti-freezing conductive gels by cononsolvency effect," *EcoMat*, vol. 3, no. 2, pp. 1–9, 2021, doi: 10.1002/eom2.12085.

[19] F. Mo, G. Liang, D. Wang, Z. Tang, H. Li, and C. Zhi, "Biomimetic organohydrogel electrolytes for high-environmental adaptive energy storage devices," *EcoMat*, vol. 1, no. 1, pp. 1–12, 2019, doi: 10.1002/eom2.12008.

[20] Y. Wang and Y. Chen, "A flexible zinc-ion battery based on the optimized concentrated hydrogel electrolyte for enhanced performance at subzero temperature," *Electrochim. Acta*, vol. 395, p. 139178, 2021, doi: 10.1016/j.electacta.2021.139178.

[21] Y. Zhu *et al.*, "Concentrated dual-cation electrolyte strategy for aqueous zinc-ion batteries," *Energy Environ. Sci.*, vol. 14, no. 8, pp. 4463–4473, 2021, doi: 10.1039/d1ee01472b.

[22] Z. Pei *et al.*, "A Flexible Rechargeable Zinc–Air Battery with Excellent Low-Temperature Adaptability," *Angew. Chemie - Int. Ed.*, vol. 59, no. 12, pp. 4793–4799, 2020, doi: 10.1002/anie.201915836.

[23] N. Sun, F. Lu, Y. Yu, L. Su, X. Gao, and L. Zheng, "Alkaline Double-Network

Hydrogels with High Conductivities, Superior Mechanical Performances, and Antifreezing Properties for Solid-State Zinc-Air Batteries," *ACS Appl. Mater. Interfaces*, vol. 12, no. 10, pp. 11778–11788, 2020, doi: 10.1021/acsami.0c00325.

[24] R. Chen *et al.*, "A Flexible and Safe Aqueous Zinc-Air Battery with a Wide Operating Temperature Range from -20 to 70 °C," *ACS Sustain. Chem. Eng.*, vol. 8, no. 31, pp. 11501–11511, 2020, doi: 10.1021/acssuschemeng.0c01111.

[25] C. Xie, Y. Li, Q. Wang, D. Sun, Y. Tang, and H. Wang, "Issues and solutions toward zinc anode in aqueous zinc-ion batteries: A mini review," *Carbon Energy*, vol. 2, no. 4, pp. 540–560, 2020, doi: 10.1002/cey2.67.

[26] Z. Yi, G. Chen, F. Hou, L. Wang, and J. Liang, "Strategies for the Stabilization of Zn Metal Anodes for Zn-Ion Batteries," *Adv. Energy Mater.*, vol. 11, no. 1, pp. 1–31, 2021, doi: 10.1002/aenm.202003065.

[27] S. Sen Chi *et al.*, "Lithiophilic Zn Sites in Porous CuZn Alloy Induced Uniform Li Nucleation and Dendrite-free Li Metal Deposition," *Nano Lett.*, vol. 20, no. 4, pp. 2724–2732, 2020, doi: 10.1021/acs.nanolett.0c00352.

[28] Y. Liu *et al.*, "Engineering integrated structure for high-performance flexible zinc-ion batteries," *Chem. Eng. J.*, vol. 417file://, no. November 2020, 2021, doi: 10.1016/j.cej.2020.127955.

[29] S. Liu, R. Zhang, J. Mao, Y. Zhao, Q. Cai, and Z. Guo, “From room temperature to harsh temperature applications: Fundamentals and perspectives on electrolytes in zinc metal batteries,” *Sci. Adv.*, vol. 8, no. 12, p. eabn5097, 2022, doi: 10.1126/sciadv.abn5097.

[30] L. Li *et al.*, “High-performance dual-ion Zn batteries enabled by a polyzwitterionic hydrogel electrolyte with regulated anion/cation transport and suppressed Zn dendrite growth,” *J. Mater. Chem. A*, vol. 9, no. 43, pp. 24325–24335, 2021, doi: 10.1039/d1ta08127f.

[31] P. Liu, R. Lv, Y. He, B. Na, B. Wang, and H. Liu, “An integrated, flexible aqueous Zn-ion battery with high energy and power densities,” *J. Power Sources*, vol. 410–411, no. November 2018, pp. 137–142, 2019, doi: 10.1016/j.jpowsour.2018.11.017.

[32] Y. Liu *et al.*, “Engineering integrated structure for high-performance flexible zinc-ion batteries,” *Chem. Eng. J.*, vol. 417, no. November 2020, 2021, doi: 10.1016/j.cej.2020.127955.